DMD Fast Forward. Published on April 20, 2017 as DOI: 10.1124/dmd.117.075226
This article has not been copyedited and formatted. The final version may differ from this version.

In Vitro Metabolism of Oprozomib, an Oral Proteasome Inhibitor: Role of Epoxide Hydrolases and Cytochrome P450s

Zhican Wang, Ying Fang, Juli Teague, Hansen Wong, Christophe Morisseau, Bruce D. Hammock, Dan A. Rock, Zhengping Wang

Department of Pharmacokinetics and Drug Metabolism (Z.W., Y.F., D.R., and Z.W.), and Clinical Pharmacology Modeling & Simulation (H.W.), Amgen Inc., South San Francisco, CA 94080

Drug Metabolism and Pharmacokinetics (J.T.), Onyx Pharmaceuticals, an Amgen Subsidiary, South San Francisco, CA 94080

Department of Entomology and Nematology (C.M., and B.H.), and UC Davis Comprehensive Cancer Center, University of California, Davis, One Shields Avenue, Davis, California 95616

DMD Fast Forward. Published on April 20, 2017 as DOI: 10.1124/dmd.117.075226
This article has not been copyedited and formatted. The final version may differ from this version.

Running Title Page

Running title: Metabolism of oprozomib by microsomal epoxide hydrolase

Corresponding author:

Zhengping Wang, PhD, Department of Pharmacokinetics and Drug Metabolism, Amgen Inc., South San Francisco, CA 94080. Phone: 650-766-6695; Email: zwang687@gmail.com

Number of text pages: 25

Number of tables: 1

Number of figures: 7

Number of supplemental tables: 1

Number of supplemental figures: 3

Number of references: 48

Number of words in the Abstract: 249

Number of words in the Introduction: 733

Number of words in the Discussion: 1492

Abbreviations

1-ABT: 1-aminobenzotriazole; BSA: bovine serum albumin; CYP: cytochrome P450; DDI: drug-drug interaction; DMSO: dimethyl sulfoxide; EH: epoxide hydrolase; FA: formic acid; GSH: glutathione; HLM: human liver microsome; IS: internal standard; LC: liquid chromatography; mEH: microsomal epoxide hydrolase; MM: multiple myeloma; MS: mass spectrometer; NSPA: 2-nonylsulfanyl-propionamide; PDA: photodiode array detector; PK: pharmacokinetics; RRMM: relapsed or/and refractory multiple myeloma; sEH: soluble epoxide hydrolase; *cis*-SO: *cis*-stilbene oxide; *trans*-SO: *trans*-stilbene oxide; TPPU: 1-trifluoromethoxyphenyl-3-(1-propionylpiperidin-4-yl) urea; UPLC-MS/MS: ultra-performance liquid chromatography tandem mass spectrometry

Abstract

Oprozomib is an oral proteasome inhibitor currently under investigation in patients with hematologic malignancies or solid tumors. Oprozomib elicits potent pharmacological actions by forming a covalent bond with the active site *N*-terminal threonine of the 20S proteasome. Oprozomib has a short half-life across preclinical species and in patients due to systemic clearance via metabolism. Potential for drug-drug interactions (DDIs) could alter the exposure of this potent therapeutic therefore a thorough investigation of pathways responsible for metabolism is required. In the present study, the major drug-metabolizing enzyme responsible for oprozomib metabolism was identified *in vitro*. A diol of oprozomib was found to be the predominant metabolite in human hepatocytes, which formed via direct epoxide hydrolysis. Using recombinant epoxide hydrolases (EHs) and selective EH inhibitors in liver microsomes, microsomal EH (mEH) but not soluble EH (sEH), was found to be responsible for oprozomib diol formation. Co-incubation with 2-nonylsulfanyl-propionamide, a selective mEH inhibitor, resulted in a significant decrease in oprozomib disappearance (>80%) with concurrent complete blockage of diol formation in human hepatocytes. On the contrary, a selective sEH inhibitor did not affect oprozomib metabolism. Pre-treatment of hepatocytes with the *pan*-CYP inhibitor 1-aminobenzotriazole resulted in a modest reduction (~20%) of oprozomib metabolism. These findings indicated that mEH plays a predominant role in oprozomib metabolism. Further studies may be warranted to determine whether drugs that are mEH inhibitors cause clinically significant DDIs with oprozomib. On the other hand, pharmacokinetics of oprozomib is unlikely to be affected by co-administered CYP and sEH inhibitors and/or inducers.

DMD Fast Forward. Published on April 20, 2017 as DOI: 10.1124/dmd.117.075226
This article has not been copyedited and formatted. The final version may differ from this version.

Introduction

The proteasome is a multicatalytic enzyme complex and key to the ubiquitin dependent pathway for intracellular protein degradation (Kisselev and Goldberg, 2001; Ciechanover, 2005). The highly regulated ubiquitin proteasome system affects a wide variety of cellular processes and is critical for cellular homeostasis. Inhibition of proteasome leads to accumulation of misfolded proteins and the induction of cell cycle arrest and apoptosis. Transformed cells, particularly multiple myeloma (MM) cells, possess elevated levels of proteasome activity. Consequently, these actively proliferating malignant cells are more sensitive to proteasome inhibitors than normal cells (Kumatori et al., 1990; Loda et al., 1997; Li and Dou, 2000; Almond and Cohen, 2002). Proteasome inhibition has emerged as an effective therapeutic strategy for the treatment of MM and some lymphomas. Bortezomib (Velcade®), the first generation proteasome inhibitor, was approved in 2003 (Bross et al., 2004; Chauhan et al., 2005; O'Connor et al., 2005). Carfilzomib (Kyprolis®), a peptide epoxyketone (Figure 1), represents a new generation of proteasome inhibitors. It selectively binds to the *N*-terminal threonine of the proteasome via two covalent bonds to form a morpholino ring (Harshbarger et al., 2015), and has demonstrated favorable clinical safety and efficacy profiles compared to bortezomib (Kuhn et al., 2007). Carfilzomib has been approved for use as a single agent and in combination with lenalidomide and dexamethasone in patients with relapsed or/and refractory multiple myeloma (RRMM) (Thompson, 2013). Notably, carfilzomib in combination with dexamethasone has doubled progression-free survival in patients with RRMM compared to bortezomib and dexamethasone in the Phase 3 ENDEAVOR clinical trial (Dimopoulos et al., 2016). The introduction of proteasome inhibitors and immunomodulatory drugs has revolutionized MM treatment with the current overall survival of MM patients increased by 2-3 fold (Anderson, 2013).

The success of bortezomib and carfilzomib has inspired efforts to develop oral proteasome inhibitors with improved flexibility in dose administration, specifically oral administration, for improved patient compliance and convenience. Ixazomib (Ninlaro®) and oprozomib, representing peptide boronate and peptide epoxyketone, respectively, are two orally bioavailable proteasome inhibitors under clinical investigation (Rajan and Kumar, 2016). Ixazomib in combination with lenalidomide and dexamethasone

administrated once-weekly demonstrated efficacy in a Phase 3 study (Moreau et al., 2016). Oprozomib (Figure 1) is being evaluated in Phase 1/2 clinical trials in patients with hematological malignancy or solid tumors (Infante et al., 2016). Similar to carfilzomib, oprozomib inhibits primarily the chymotrypsin-like activity of the constitutive and immunoproteasomes via covalent modification of the *N*-terminal threonine (Zhou et al., 2009). It has shown promising clinical activity in patients with RRMM either as a single agent or in combination with pomalidomide and dexamethasone (Hari et al., 2015; Shah et al., 2015; Vij et al., 2015).

Oprozomib is a tripeptide analogue (Figure 1) of carfilzomib that was developed to improve absorption. It was believed that smaller peptides were likely to be more effectively delivered across the small intestine (Hamman et al., 2005; Zhou et al., 2009). When dosed via oral gavage to Balb/C mice at 30 mg/kg, more than 80% proteasome inhibition was observed in blood, liver and adrenal gland one hour post administration (Zhou et al., 2009). Furthermore, oprozomib demonstrated improved metabolic stability *in vitro* across multiple species compared to carfilzomib. Nonetheless, oprozomib still displayed high systemic clearance and short half-life (Fang et al., 2015). This is not surprising because both the peptide backbone and the epoxyketone warhead could be susceptible to metabolism (Yang et al., 2011; Wang et al., 2013). The rapid clearance of oprozomib was primarily mediated by metabolism, supported by the observation that parent compound was a minor component in urine and bile samples from rats, as well as urine samples from human (in-house unpublished data). In addition, oprozomib has shown a relatively large inter-patient pharmacokinetic (PK) variability (Infante et al., 2016).

The objective of the present study was to characterize the major metabolic pathways and key enzymes responsible for oprozomib metabolism *in vitro* using cryopreserved human hepatocytes, recombinant enzymes, and liver cellular fractions in the presence and absence of selective enzyme inhibitors. Deciphering the role of various enzymes responsible for oprozomib elimination is important in drug-drug interaction (DDI) risk assessment and mitigation of exaggerated pharmacology of this potent therapeutic. Particularly, it is important for CYP-mediated DDIs since CYP isoforms are responsible for the primary metabolism of the majority of small molecule drugs on the market (Wienkers and Heath,

DMD Fast Forward. Published on April 20, 2017 as DOI: 10.1124/dmd.117.075226
This article has not been copyedited and formatted. The final version may differ from this version.

2005). Defining the primary metabolic routes could also help shed light on the observed oprozomib PK variabilities in patients.

Materials and Methods

Materials. All chemicals and reagents were obtained from Sigma (St. Louis, MO) and liquid chromatography (LC) solvents were obtained from Fisher Scientific (Pittsburgh, PA). Oprozomib and authentic metabolite standards were synthesized and characterized at Onyx Pharmaceuticals, an Amgen subsidiary (South San Francisco, CA). Deuterated oprozomib (d5-oprozomib, five deuterium on the benzyl ring) was obtained from PepTech Corp (Bedford, MA). A selective mEH inhibitor, 2-nonylsulfanyl-propionamide (NSPA) was previously synthesized (Morisseau et al., 2008), and a selective sEH inhibitor 1-trifluoromethoxyphenyl-3-(1-propionylpiperidin-4-yl) urea (TPPU) was previously characterized (Rose et al., 2010). The structures of these two inhibitors are shown in Supplemental Figure 1. Human recombinant microsomal epoxide hydrolase (mEH, # Cri 08.17, purity 80%) and soluble epoxide hydrolase (sEH, # Cri 71.16, purity 95%) were prepared and characterized as described previously (Morisseau et al., 2000; Morisseau et al., 2011). Supersomes containing cDNA-expressed human CYPs, CYP reductase and cytochrome b5 were purchased from BD Bioscience (San Jose, CA). Pooled human cryopreserved hepatocytes (Lot# FDX, 20 donors, mixed gender) and media were purchased from BioreclamationIVT (Baltimore, MD). Liver subcellular fractions including male or female liver microsomes, and cytosols (10 donors per gender, age: 21 – 58) were purchased from Sekisui Xenotech (Kansas City, KS). Pooled, gender mixed liver microsomes were prepared by mixing an equal volume of male (10 donors) and female (10 donors) liver microsomes.

Metabolic profiling of oprozomib in human hepatocytes. Pooled cryopreserved human hepatocytes were thawed at 37 °C, centrifuged at 65 g in 45 ml thawing medium, and re-suspended in maintenance medium. Cell viability and density were measured by a trypan blue exclusion assay. For metabolic profiling, suspensions (1.0 ml) containing hepatocytes (0.5 million cells/ml) were incubated with 10 µM of oprozomib for 1 hour. Reactions were conducted in 37 °C cell culture incubator with 100% relative humidity, 95% air, 5% CO_2. Final incubation contained 0.2% of dimethyl sulfoxide (DMSO). Reactions

DMD Fast Forward. Published on April 20, 2017 as DOI: 10.1124/dmd.117.075226
This article has not been copyedited and formatted. The final version may differ from this version.

were terminated by addition of an equal volume of acetonitrile with 0.1% formic acid (FA). Control incubation was prepared as follow: a mixture containing hepatocytes only was incubated for 1 hour, quenched with acetonitrile with 0.1% FA, and then spiked with 10 µM of oprozomib. Supernatants (600 µl) were concentrated under a nitrogen stream and then reconstituted in 100 µl of 40% acetonitrile/water (0.1% FA). Metabolite identification was conducted using a Thermo Oribtrap Q Exactive high-resolution mass spectrometer (MS) equipped with a Thermo Accela LC system. Metabolite structures were assigned based on the accurate mass obtained from a full scan mode at a resolution of 70,000 and MS^2 fragmentation pattern from data-dependent acquisition at a resolution of 17,500. For the quantification of oprozomib diol and PR-025 [(*S*)-2-amino-1-((*R*)-2-methyloxiran-2-yl)-3-phenylpropan-1-one] diol formation in human hepatocytes, cells (0.25 ml, 0.5 million cells/ml) were incubated with 2 µM of oprozomib in 12-well, collagen-coated plates (Thermo Scientific, CA). At each time point (0, 10, 20, 30, and 60 min), reactions were terminated by the addition of an equal volume of acetonitrile containing 100 ng/ml internal standard (IS) d_5-oprozomib. After centrifugation, supernatants were collected and analyzed for oprozomib and the major metabolites by LC-MS/MS as described below.

Epoxide hydrolysis by recombinant human mEH and sEH *in vitro*. Recombinant human EHs were kept at -80 °C until use. Briefly, incubations (0.1 ml) were conducted in 0.1 M Tris-HCl buffer (pH 9.0 for mEH; pH 7.5 for sEH) containing 0.1 mg/ml fatty acid-free bovine serum albumin (BSA) (Morisseau et al., 2000; Morisseau et al., 2011). Enzyme activities of mEH and sEH (5 µg/ml) towards epoxide hydrolysis were confirmed using their corresponding probe substrates (50 µM) *cis*-stilbene oxide (*cis*-SO) and *trans*-stilbene oxide (*trans*-SO), respectively. In order to determine whether oprozomib is a substrate for recombinant mEH or/and sEH, enzymes were pre-warmed for 5 min at 37 °C before the addition of oprozomib (2 µM) to initiate the reaction. The enzyme concentration used was from 1 – 10 µg/ml for mEH, and up to 100 µg/ml for sEH. After 0, 10, 20 or 30 min as indicated, reactions were terminated by addition of 2 volumes of acetonitrile containing 0.1% FA and supernatants were collected for LC-MS/MS analysis.

DMD Fast Forward. Published on April 20, 2017 as DOI: 10.1124/dmd.117.075226
This article has not been copyedited and formatted. The final version may differ from this version.

Kinetics of oprozomib epoxide hydrolysis in recombinant mEH and human liver microsomes (HLMs). Reaction kinetic parameters (V_{max} and K_m) were determined using recombinant mEH (2 μg/ml, calculated based on 80% purity), oprozomib (10 – 600 μM) in 0.1 M Tris-HCl buffer (pH 9.0) containing 0.1 mg/ml BSA. Kinetic studies in male and female HLMs, were conducted in 0.1 M potassium phosphate buffer (pH 7.4) containing 0.1 mg/ml BSA. The final microsomal protein concentration was optimized to be 0.5 mg/ml and oprozomib was 10 – 600 μM. The final DMSO concentration was 0.5%. Oprozomib was added to initiate the reaction after pre-warming enzymes for 5 min. Incubations (0.2 ml) were conducted at 37 °C for 30 min and terminated by addition of 2 volumes of acetonitrile containing 100 ng/ml of IS d5-oprozomib. For kinetic studies of *cis*-SO, incubations (0.4 ml) were optimized and performed using 4 μg/ml recombinant mEH or 0.1 mg/ml microsomal proteins, and *cis*-SO (1 – 200 μM) at 37 °C for 10 min. The reaction was terminated by addition of one volume acetonitrile containing 50 μM *trans*-SO as IS. Supernatants were collected by centrifugation and analyzed by either UPLC-MS/MS or UPLC linked with a photodiode array detector (PDA) as described below. Each set of data was fit to a simple Michaelis-Menten kinetics model using nonlinear regression data analysis (GraphPad Prism v.6). Each experimental reaction condition was conducted in triplicate.

NSPA was used as the selective mEH inhibitor to inhibit mEH enzyme activities in HLMs (Morisseau et al., 2008). Briefly, pre-warmed pooled HLMs (0.5 mg/ml) were incubated with oprozomib (10 μM) in the absence or presence of NSPA (0.02 – 100 μM) in 0.1 M potassium phosphate buffer (pH 7.4, 0.1 mg/ml BSA) at 37 °C. After 15 min, reactions were quenched with 2 volumes of acetonitrile containing 0.1% FA and supernatants were isolated for quantitative analysis. The inhibitory effects of NSPA on *cis*-SO (50 μM) hydrolysis were also determined under the similar conditions except for a lower microsomal protein concentration (0.1 mg/ml) and shorter incubation time (10 min). The IC_{50} values were estimated using nonlinear regression data analysis (GraphPad Prism v.6).

Inhibition of oprozomib epoxide hydrolysis in human hepatocytes in the presence of EH inhibitors. Pooled cryopreserved human hepatocytes were thawed out and re-suspended in hepatocyte maintenance medium, and cell viability and density were measured. Incubation mixtures (0.1 ml) contained human

hepatocytes (0.5 million cells/ml), oprozomib (2 μM) or *cis*-SO (50 μM), and inhibitors NSPA or TPPU (10 μM). The final solvent DMSO concentration was 0.2%. At each time point (0, 2, 5, 10, 20, 40, and 60 min), reactions were terminated by the addition of 2 volumes of acetonitrile containing IS either d_5-oprozomib or *trans*-SO. After centrifugation, supernatants (150 μl) were collected and analyzed using LC-MS/MS or LC-PDA as described below.

Inhibition of CYP-mediated oprozomib metabolism in human hepatocytes by 1-aminobenzotriazole (1-ABT). The role of CYPs on oprozomib metabolism in human hepatocytes was investigated using a *pan*-CYP inhibitor 1-ABT. Pooled cryopreserved human hepatocytes were thawed at 37 °C, centrifuged and re-suspended in hepatocyte maintenance medium. Incubations (0.25 ml) containing hepatocytes (0.5 million cells/ml) were pre-incubated with 0.5 mM 1-ABT or solvent (0.1% DMSO) for 30 min. Oprozomib was added at a final concentration of 2 μM to initiate the reactions. Reactions were conducted in a 37 °C cell culture incubator with 100% relative humidity, 95% air, 5% CO_2. At each time point (0, 2, 5, 10, 20, 40, and 60 min), reactions were terminated by the addition of an equal volume of acetonitrile containing IS d_5-oprozomib. After centrifugation, supernatants were collected for the quantification of oprozomib disappearance and PR-176 formation by LC-MS/MS.

Metabolic stability of oprozomib in HLMs and recombinant CYPs. Metabolic stability of oprozomib in pooled HLMs (mixed gender) was conducted in the presence and absence of cofactor NADPH. The value of intrinsic clearance was determined by the rate of parent compound disappearance (Obach, 1999). Briefly, oprozomib (1 μM) was mixed with liver microsomes (0.25 mg/ml) with or without 1 mM NADPH in 0.1 M potassium phosphate buffer (pH7.4) containing 3.3 mM of $MgCl_2$. The incubation mixtures were kept at 37 °C for 1, 5, 10, 20, 30, and 40 min. The disappearance of oprozomib was monitored using a LC-MS/MS method described below. In addition, a preliminary *in vitro* CYP phenotyping study was conducted by incubating oprozomib (1 μM) with six major recombinant CYP isoforms (125 pmol/ml) 1A2, 2D6, 3A4, 2C8, 2C9 and 2C19 individually, in the presence of 1 mM NADPH at 37 °C for 0, 15, 30, and 60 min. The percentage of oprozomib remaining after incubation was calculated by comparing the peak response with that from the zero-minute incubation.

DMD Fast Forward. Published on April 20, 2017 as DOI: 10.1124/dmd.117.075226
This article has not been copyedited and formatted. The final version may differ from this version.

Inhibition of CYP activities by oprozomib. The relative potential of oprozomib to inhibit 6 major CYP isoforms was assessed in pooled HLMs (mixed gender) with and without a 30 min pre-incubation. The probe substrates used were phenacetin (CYP1A2), amodiaquine (CYP2C8), diclofenac (CYP2C9), *S*-mephenytoin (CYP2C19), dextromethorphan (CYP2D6), midazolam and testosterone (CYP3A4/5). The incubation mixtures (0.2 ml) contained oprozomib with various concentrations (0 – 30 μM), a probe substrate, microsomal proteins and 1.5 mM NADPH in 0.1 M potassium phosphate buffer (pH 7.4) with 3 mM $MgCl_2$ for 15 min. To examine time-dependent inhibition, oprozomib was pre-incubated with liver microsomes for 30 min in the presence of NADPH, followed by the addition of probe substrates. The concentrations of CYP probe substrates were approximately equal to their reported K_m values. The microsomal protein concentration was 0.05 or 0.1 mg/ml. The low protein concentrations were chosen to minimize possible binding of oprozomib to microsomal proteins or lipids, as well as reduce oprozomib metabolism via epoxide hydrolysis.

Quantification of oprozomib and its metabolites using LC-MS/MS. Quantification of oprozomib and its major metabolites was performed using either an AB Sciex QTrap 4500 or 5500 MS equipped with an electrospray ionization source. Chromatographic separation was achieved using a Waters XBridge BEH C18 column (3.5 μ, 2.1 mm × 50 mm) and water (A)-acetonitrile (B) containing 0.1% FA as mobile phases at a flow rate of 0.5 ml/min. The mobile phase started at 10% B for 0.5 min, and linearly increased to 65% B within 1 min, held for 0.3 min before increasing to 95% B within 0.2 min, hold at 95% B for 1.5 min and returned to 10% B within 0.2 min. Multiple reaction monitoring of the transitions *m/z* 533.0 -> 126.0, 551.3 -> 325.2, 206.0 -> 120, 224.0 -> 150.0, and 538.2 -> 126.1 was used to detect oprozomib, PR-176, PR-025, PR-025 diol, and IS d_5-oprozomib, respectively. Calibration curves were generated by plotting the peak area ratio for each compound and IS versus the corresponding concentrations of synthetic metabolite standards, and fitting with a linear regression equation.

Quantification of *cis*-SO, *trans*-SO, *R,R*-hydroxybenzoin and *meso*-hydroxybenzoin using LC-PDA. Formation of *R,R*-hydroxybenzoin and *meso*-hydroxybenzoin from *cis*-SO and *trans*-SO hydrolysis was used for measuring mEH and sEH activities *in vitro*, respectively. Quantification of these two diol

products was performed using a Shimadzu LC-20AD system coupled with a PDA detector. Chromatographic separation was achieved using a Waters XBridge BEH C18 column (2.1 mm × 100 mm, 3.5 μm) and water (A)-acetonitrile (B) containing 0.1% FA as mobile phases at a flow rate of 0.3 ml/min. The mobile phase started at 10% B for 0.5 min, and linearly increased to 95% B at 5 min, hold for 2 min before returning to initial 10% B within 0.5 min. The total running time was 9 min. Quantification of the diol metabolites was calculated by fitting their peak area ratio (metabolites/IS) to the calibration curves which generated by using authentic metabolite standards *R,R*-hydroxybenzoin and *meso*-hydroxybenzoin, respectively.

Statistical analysis. GraphPad Prism v. 6 (GraphPad Software Inc., La Jolla, CA) was used for the statistical analysis. Data represent mean ± S.D.. The means of the measured values of each treatment group were compared using Student's t-test. Means were considered statistically different from one another if $p < 0.05$.

Results

Oprozomib metabolism in human hepatocytes. Incubation in cryopreserved human hepatocytes with oprozomib for 60 min led to the formation of several metabolites, which were detected by LC-MS/MS (Figure 2). A diol of oprozomib (also known as PR-176) was formed from direct epoxide hydrolysis (Figure 2A). This appeared as the predominant metabolite based upon both MS ion signals and ultraviolet absorbance. A peptide bond cleavage product with *m/z* at 245.0587 (cleavage on bond 2) was also observed, albeit at relatively low levels. Another low abundance metabolite with *m/z* at 224.1276 (diol of PR-025) resulted from peptide cleavage (cleavage on bond 1) and epoxide hydrolysis was detected. In addition, multiple trace metabolites including from hydroxylation or/and de-methylation, direct GSH conjugation, and the combination of oxidation and epoxide hydrolysis or GSH conjugation, were also observed.

Quantification of oprozomib disappearance and its major metabolite formation in hepatocyte incubation was performed using synthesized standards. As shown in Figure 2B, PR-176 was readily formed after incubation with oprozomib (2 μM). After 60 min incubation, nearly 55% of total oprozomib

DMD Fast Forward. Published on April 20, 2017 as DOI: 10.1124/dmd.117.075226
This article has not been copyedited and formatted. The final version may differ from this version.

was recovered as the diol, about 7% was recovered as the diol of PR-025, and 20% remained as oprozomib. These quantitative results suggest that epoxide hydrolysis is the major metabolic pathway for oprozomib in human hepatocytes. Other minor pathways, such as peptide cleavage, oxidation and GSH conjugation, combined to contribute to the remaining 18% of oprozomib from the initial incubation. It is worth mentioning that in rat hepatocyte incubations, two oprozomib conjugates via direct GSH conjugation were identified as major metabolites, in addition to PR-176 (Supplemental Figure 2).

Oprozomib hydrolysis by recombinant human mEH but not sEH. Since epoxide hydrolysis was identified to be the major metabolic pathway, recombinant human mEH and sEH were used to investigate the capacity of the different EH isoforms to hydrolyze oprozomib epoxide. Formation of PR-176 increased linearly with both incubation time (up to 30 min, data not shown) and mEH concentration (0.5 – 10 μg/ml) as shown in Figure 3A. In contrast, no significant formation of PR-176 was observed when oprozomib was incubated with recombinant sEH for 30 min, at enzyme concentration up to 100 μg/ml. In a parallel experiment, both mEH and sEH can readily convert their corresponding probe substrates, *cis*-SO or *trans*-SO, respectively, in a time-dependent manner (Figure 3B).

The kinetics of oprozomib epoxide hydrolysis were subsequently evaluated using recombinant mEH. The highest oprozomib concentration (up to 600 μM) was chosen based on its aqueous solubility in the phosphate buffer system. An optimized protein concentration (2 μg/ml) and incubation time (30 min) were applied in the study to ensure the linearity over the course of the reaction with sufficient amounts of PR-176 formation for accurate quantification. As shown in Figure 3C, formation of PR-176 increased with oprozomib concentration up to 600 μM without reaching a plateau. Fitting the data into the Michaelis-Menten equation estimated the values of K_m and V_{max} of oprozomib at 974 ± 112 μM and 109 ± 8.6 nmol/min/mg proteins, respectively. While the values of K_m and V_{max} could not be more accurately determined under the current assay conditions, the estimation suggests a relatively high K_m for oprozomib epoxide hydrolysis with recombinant mEH. As a control, the values of K_m and V_{max} of *cis*-SO were determined to be 56.9 ± 3.8 μM and 648 ± 17 nmol/min/mg proteins, respectively, which was comparable to previously reported literature values (Morisseau et al., 2011).

DMD Fast Forward. Published on April 20, 2017 as DOI: 10.1124/dmd.117.075226
This article has not been copyedited and formatted. The final version may differ from this version.

Inhibition of oprozomib epoxide hydrolysis by a selective mEH inhibitor in HLMs. NSPA is a selective mEH inhibitor that has been previously characterized with recombinant rat and human mEH for its potency (Morisseau et al., 2008; Morisseau et al., 2011). Here, we evaluated its potency in inhibiting hydrolysis of *cis*-SO and oprozomib in HLMs. As seen in Figure 4A, NSPA significantly inhibited *cis*-SO hydrolysis with a mean IC_{50} value of 0.35 μM, and oprozomib diol formation with a mean IC_{50} value of 0.51 μM in HLMs. Kinetics of oprozomib diol formation in both male and female HLMs were also determined (Figure 4B). Similar to what was observed in the kinetic study with recombinant mEH (Figure 3), formation of PR-176 essentially increased linearly with oprozomib concentrations without reaching a plateau. As a result, the values of K_m and V_{max} could not be accurately estimated using nonlinear regression analysis. Considering the K_m values were likely over 5-fold higher than 50 μM, the apparent ratios of V_{max}/K_m were roughly calculated from the slopes of PR-176 formation rate over low oprozomib concentration range (10 – 50 μM). As a result, the mean V_{max}/K_m values were estimated as 8.43 and 3.20 μl/min/mg protein in male and female HLMs, respectively. In addition, the mean values of V_{max}/K_m towards *cis*-SO and oprozomib epoxide hydrolysis in liver microsomes from rats and dogs were also estimated (Supplemental Table 1). As a control, the estimated mean V_{max}/K_m value for *cis*-SO were comparable to what reported in literature (Kitteringham et al., 1996).

Effect of the mEH inhibitor NSPA on oprozomib metabolism in human hepatocytes. Both NSPA and TPPU were used to further determine the importance of mEH and sEH, respectively, on oprozomib metabolism in human hepatocytes (Figure 5). The metabolic stability of two inhibitors TPPU and NSPA in human hepatocytes were first determined. TPPU was stable in human hepatocytes over a one-hour incubation, whereas NSPA was labile with a half time ($t_{1/2}$) ~15 min. Thus, a concentration of NSPA (10 μM) 20-fold higher than the measured *in vitro* IC_{50} values on mEH activity was used in the human hepatocyte study. The inhibitory effect of NSPA in human hepatocytes was first confirmed using *cis*-SO as the probe substrate; over 80% inhibition of *cis*-SO hydration was observed within 10-min incubation, however, inhibition was reduced to 60% with a longer incubation time (up to 20 min) (data not shown). The rate of oprozomib metabolism in human hepatocytes was significantly inhibited (~80%) by NSPA

DMD Fast Forward. Published on April 20, 2017 as DOI: 10.1124/dmd.117.075226
This article has not been copyedited and formatted. The final version may differ from this version.

co-treatment (9.7 ± 0.9 µl/min/10^6 cells) compared to vehicle DMSO control (40.7 ± 1.4 µl/min/10^6 cells). Consistently, formation of PR-176 was also significantly decreased (>90% inhibition) by NSPA treatment up to 60-min incubation (Figure 5B). In contrast, the sEH inhibitor TPPU did not significantly inhibit oprozomib metabolism (35.0 ± 1.5 µl/min/10^6 cells) and PR-176 formation (Figure 5).

Metabolic stability of oprozomib in HLMs in the presence and absence of NADPH. Metabolic identification and quantitation results (Figure 2 & 5) in human hepatocytes have suggested a minor role of CYPs on oprozomib metabolism. HLM contains high hepatic mEH activity, and is also a common *in vitro* system for assessment of CYPs-mediated metabolism. Therefore, microsomes were expected to be a relevant *in vitro* system to study the metabolism of oprozomib. Interestingly, in pooled HLMs, the presence of NADPH significantly increased the intrinsic clearance of oprozomib by 3.5-fold, as compared to that in the absence of NADPH (70.7 ± 2.9 vs. 20.2 ± 1.8 µl/min/mg protein) (Figure 6A). These results indicated a significant role of oxidation pathways over epoxide hydrolysis for oprozomib metabolism in HLMs, which is not consistent with what was observed in human hepatocytes (Figure 2).

Oprozomib showed time-dependent inhibition of CYP3A4 in HLMs. *In vitro* inhibition potential of oprozomib on major CYP isoforms (CYP1A2, 2C8, 2C9, 2C19, 2D6 and 3A4/5) was also evaluated using pooled HLMs (Table 1). Oprozomib did not inhibit the activities of CYP1A2, 2C8, 2C9, 2C19 and 2D6 at concentrations up to 30 µM with or without a 30 min pre-incubation. Oprozomib (30 µM) reduced the activity of CYP3A4/5 by 45% and 33% as measured by testosterone 6β-hydroxylation and midazolam 1´-hydroxylation assays, respectively, without pre-incubation. The inhibitory effect was further enhanced with 30 min pre-incubation, where the IC_{50} values decreased to 12 and 5.5 µM with midazolam and testosterone as the substrate, respectively (Table 1). This time-dependent inhibition was NADPH-dependent and resistant to dilution (data not shown). The ratio of the maximum inactivation rate constant (k_{inact}) to the concentration of the inactivator that gives half the maximum rate of inactivation (K_I) was about 2.0 and 1.4 ml/min/µmol, respectively, with midazolam and testosterone as marker substrates. In addition, a preliminary CYP phenotyping study using recombinant CYP isoforms showed oprozomib was a substrate of CYP3A4 (Figure 6B).

DMD Fast Forward. Published on April 20, 2017 as DOI: 10.1124/dmd.117.075226
This article has not been copyedited and formatted. The final version may differ from this version.

Effect of the *pan*-CYP inhibitor 1-ABT on oprozomib metabolism in human hepatocytes. In this experiment, the rates of oprozomib metabolism in human hepatocytes in the absence and presence of a *pan*-CYP inhibitor 1-ABT were compared. After pre-incubation with 1-ABT (0.5 mM) to inactivate CYP enzymes (in control experiments, 1-ABT reduced testosterone oxidation by 90%), oprozomib disappearance was modestly reduced by ~20% (clearance with 1-ABT: 31.6 ± 1.4 μl/min/10^6 cells; without 1-ABT: 41.8 ± 1.2 μl/min/10^6 cells) (Figure 7A). As expected, 1-ABT did not affect the formation of PR-176 (Figure 7B). In addition, pre-treatment of hepatocytes with 0.5 mM 1-ABT completely blocked the formation of oprozomib metabolites from direct CYP-mediated oxidation, as well as secondary products through oxidation and epoxide hydrolysis as shown in Figure 2.

Discussion

Peptide epoxyketone drugs represent a new class of proteasome inhibitors that are highly efficacious for the treatment of patients with MM. As these inhibitors act via covalent modification, they induce prolonged pharmacodynamic effects in spite of a short duration of systemic exposure (Yang et al., 2011; Wang et al., 2013). Proteasome activity recovery primarily relies on the rate of *de novo* proteasome synthesis, with a half-life of about 20-72 hours across a variety of tissues in preclinical species, except for blood after dosing with oprozomib (Zhou et al., 2009; Dou and Zonder, 2014). Different from the first generation epoxyketone proteasome inhibitor carfilzomib, which is administered intravenously due to the lack of oral bioavailability, oprozomib demonstrated improved metabolic stability and was orally bioavailable (Zhou et al., 2009). Yet, oprozomib still displayed high systemic clearance, a short half-life and relatively high PK variability in preclinical species and patients (Fang et al., 2015; Infante et al., 2016).

To understand the parameters governing the elimination of oprozomib, a number of *in vitro* metabolism studies were conducted. As summarized in Scheme 1, the *in vitro* metabolism data showed that hydrolysis of oprozomib epoxide to form the diol PR-176 by EH is the major metabolic pathway in human hepatocytes, with peptide cleavage by peptidases, oxidation by CYPs, and direct GSH conjugation representing minor alternative metabolic pathways. Consistent with the results in human hepatocytes,

PR-176 was also found to be a major circulating metabolite in dogs, the non-rodent toxicity species, as well as human plasma samples from a first-in-human clinical study (in-house unpublished data). Interestingly, GSH conjugation, an alternative pathway to detoxify xenobiotic epoxides, was minor in human hepatocytes. Although cryopreservation may reduce the *in vitro* GSH-conjugating capacity in both human and rat hepatocytes (Sohlenius-Sternbeck and Schmidt, 2005), two GSH conjugates of oprozomib were identified as major metabolites in addition to diol in cryopreserved rat hepatocytes. In addition, multiple GSH conjugates were observed for clozapine, a positive control for GSH adduct formation in both rat and human hepatocytes (Supplemental Figure 3). Consistent with the *in vitro* observation, no detectable GSH conjugates were observed in human plasma and urine samples; on the other hands, GSH conjugates were observed *in vivo* in rat plasma samples (in-house unpublished data). These data indicate GSH conjugation plays a minor role in oprozomib metabolism in humans.

The predominant role of EHs on oprozomib metabolism could have implications on potential of DDI and therefore may influence development strategy. Several EHs are found in mammals, among them, two major isoforms, mEH and sEH, have been extensively characterized (Fretland and Omiecinski, 2000; Kodani and Hammock, 2015). Both isoforms are expressed ubiquitously throughout the mammalian body with the highest expression generally in the liver (Gill and Hammock, 1980; Pacifici et al., 1988; Coller et al., 2001). Collectively, data from recombinant EHs (Figure 3), liver microsomes (Figure 4) and hepatocytes in the presence or absence of selective inhibitors (Figure 5) indicate that the epoxide ring opening of oprozomib was catalyzed by mEH, but not sEH. Therefore, oprozomib PK is unlikely to be affected by the co-administration with sEH inhibitors. On the other hand, oprozomib is primarily metabolized by mEH, and amide-containing drugs such as valpromide or progabide have been shown to inhibit *in vivo* mEH activity (Fretland and Omiecinski, 2000; Kodani and Hammock, 2015). Thus, further studies may be warranted to determine whether drugs that are mEH inhibitors cause clinically significant drug-drug interactions with oprozomib. Moreover, mEH is involved in the metabolism of numerous xenobiotics, including 1,3-butadiene, naphthalene, carbamazepine and phenytoin (Decker et al., 2009). It is possible that oprozomib acts as a mEH inhibitor that affects the

clearance of co-administered drugs which are mainly metabolized by mEH. However, a preliminary *in vitro* study in human liver microsomes showed that oprozomib does not significantly inhibit *cis*-SO epoxide hydrolysis at a concentration up to 100 µM (data not shown).

The high variability of oprozomib PK observed in preclinical species and patients could be attributed to variability of absorption and/or metabolism by mEH. Expression of mEH in ex vivo tissues was shown to vary considerably among individuals (up to 8-fold) (Hassett et al., 1997), and that expression is affected by age, sex, diseases, and environmental factors (Vaclavikova et al., 2015). In addition, two human polymorphisms have been identified in the coding region of the mEH gene: exon 3 (a Tys113His mutation) resulting in a 50% decrease in enzyme activity *in vitro* and exon 4 (a His139Arg mutation) resulting in a 25% increase in enzyme activity *in vitro* (Pinarbasi et al., 2010). The variant alleles, however, appeared to exert only a modest impact on mEH enzymatic activities (within two fold) *in vivo* (Kroetz et al., 1993; Hosagrahara et al., 2004). Based on this information and the high systemic clearance of oprozomib, inter-individual difference in mEH activity may contribute to the high inter-individual PK variability of oprozomib in patients (Infante et al., 2016), but it is unlikely to be the main factor. Variable absorption, particularly associated with a narrow absorption window, may be another a key factor to oprozomib PK variability (Teague et al., 2013).

In contrast to the major role of mEH, a minor role of CYP on oprozomib metabolism was observed in human hepatocytes (Figure 7). Using the *pan*-CYP inhibitor 1-ABT, a modest decrease in oprozomib disappearance (< 20%) was observed. This corroborates the result that oxidative products are minor metabolites in human hepatocytes (Figure 2), as well as in plasma samples from patients (in-house unpublished data). Thus, although oprozomib is a substrate of CYP3A4, co-administration of oprozomib with other drugs that are CYP modulators would be unlikely to significantly alter the PK of oprozomib. In addition, oprozomib did display time-dependent inhibition of CYP3A4/5 in HLMs (Figure 6), however, the inhibitory effect was not manifested *in vivo* in a clinical DDI study where oprozomib was administered orally and co-administered with midazolam (Tsimberidou et al., 2016).

Choosing relevant *in vitro* systems is critical in understanding the metabolism and associated DDI potentials for oprozomib and other peptide epoxyketone inhibitors. When studying oprozomib metabolism in HLMs (Figure 6), a higher level of CYP-mediated metabolism was observed in contrast to the results observed in human hepatocytes (Figure 7). Moreover, the high level of oxidative metabolites in HLMs were also not consistent with the *in vivo* human metabolite profiling results (in-house unpublished data). The distinct observation of oprozomib metabolism in HLMs vs. human hepatocytes might be due to a significant loss of mEH activity during microsomal subcellular fractionation. In hepatocytes, beside endoplasmic reticulum membrane, mEH is also present on the plasma membrane facing the extracellular medium (Levy, 1996), thus a significant portion of the hepatocyte mEH activity might be lost when preparing microsomes. On the other hand, CYP activities are concentrated in endoplasmic reticulum membrane, which could explain why HLM incubation may bias metabolism toward CYP oxidation.

Furthermore, it is worth discussing the limitations of using hepatocytes in evaluation of the metabolism and extrapolation of the *in vivo* clearance of peptide epoxyketone analogues. Hepatocytes provided consistent metabolic profiles for oprozomib with those from *in vivo* samples. However, the rates of oprozomib disappearance and diol formation from *in vitro* hepatocyte incubation would under-predict the *in vivo* clearance of oprozomib, which was measured higher than hepatic blood flow in preclinical species (Fang et al., 2015). There are several possible reasons. First, the rate of diol formation obtained from *in vitro* kinetic incubation may underestimate the efficiency of mEH. For EH-mediated hydrolysis, the epoxide is rapidly trapped as a covalent hydroxyl alkyl enzyme intermediate. The rate of diol formation is limited by the slow hydrolysis of the intermediate (Armstrong, 1999). Second, the activity of epoxide hydrolases is generally not well characterized in commercial preparations. The effects of reagents and *in vitro* preparation procedure on epoxide hydrolase activity have not been systematically studied to the best of our knowledge. Third, extrahepatic metabolism also plays an important role in the elimination of this series of compounds because EHs and peptidases are ubiquitously expressed throughout the body. Therefore, the rate of metabolism in hepatocytes could be used simply as a tool to

rank order analogues for prioritizing in vivo studies instead of extrapolating clearance during lead optimization.

In summary, *in vitro* characterization of oprozomib metabolism revealed that epoxide hydrolysis mediated by mEH, rather than sEH, is the major metabolic pathway for oprozomib metabolism, consistent with findings from *in vivo* samples. Oxidative metabolism plays a minor role in oprozomib elimination. These data suggest CYP and sEH activity modulators when co-administered with oprozomib would unlikely significantly affect oprozomib PK. On the contrary, the results in the present study indicate that mEH inhibitors administered concomitantly with oprozomib may affect oprozomib PK. Further studies may be warranted to determine whether drugs that are mEH inhibitors cause clinically significant DDIs with oprozomib. Hepatocytes serve as a good *in vitro* system to assess the metabolic profiles of peptide epoxyketone inhibitors but generally under-estimate the rate of *in vivo* clearance of oprozomib. Metabolic findings using liver microsomes should be interpreted with caution as the microsomal system may be biased toward CYP-mediated metabolism and underestimates non-CYP metabolism for peptide epoxyketones.

Acknowledgement

We thank to Drs. Larry Wienkers, Ji Ma, Brooke Rock, and Lixia Jin from the Department of Pharmacokinetics and Drug Metabolism, Amgen Inc. for reviewing the manuscript and helpful suggestions on study design and data analysis.

Authorship Contributions

Participated in research design: Wang, Fang, and Wang

Conducted experiments: Wang, Fang, Teague, and Wong

Contributed new reagents or analytic tools: Morisseau, Hammock

Performed data analysis: Wang, Fang, Teague, Wong, Morisseau, Rock, and Wang

Wrote or contributed to the writing of the manuscript: Wang, Fang, Morisseau, Hammock, Rock, and Wang

References

Almond JB and Cohen GM (2002) The proteasome: a novel target for cancer chemotherapy. *Leukemia* **16:**433-443.

Anderson KC (2013) Therapeutic advances in relapsed or refractory multiple myeloma. *J Natl Compr Canc Netw* **11:**676-679.

Armstrong RN (1999) Kinetic and chemical mechanism of epoxide hydrolase. *Drug Metab Rev* **31:**71-86.

Bross PF, Kane R, Farrell AT, Abraham S, Benson K, Brower ME, Bradley S, Gobburu JV, Goheer A, Lee SL, Leighton J, Liang CY, Lostritto RT, McGuinn WD, Morse DE, Rahman A, Rosario LA, Verbois SL, Williams G, Wang YC, and Pazdur R (2004) Approval summary for bortezomib for injection in the treatment of multiple myeloma. *Clin Cancer Res* **10:**3954-3964.

Chauhan D, Hideshima T, Mitsiades C, Richardson P, and Anderson KC (2005) Proteasome inhibitor therapy in multiple myeloma. *Mol Cancer Ther* **4:**686-692.

Ciechanover A (2005) Intracellular protein degradation: from a vague idea, through the lysosome and the ubiquitin-proteasome system, and onto human diseases and drug targeting (Nobel lecture). *Angew Chem Int Ed Engl* **44:**5944-5967.

Coller JK, Fritz P, Zanger UM, Siegle I, Eichelbaum M, Kroemer HK, and Murdter TE (2001) Distribution of microsomal epoxide hydrolase in humans: an immunohistochemical study in normal tissues, and benign and malignant tumours. *Histochem J* **33:**329-336.

Decker M, Arand M, and Cronin A (2009) Mammalian epoxide hydrolases in xenobiotic metabolism and signalling. *Arch Toxicol* **83:**297-318.

Dimopoulos MA, Moreau P, Palumbo A, Joshua D, Pour L, Hajek R, Facon T, Ludwig H, Oriol A, Goldschmidt H, Rosinol L, Straub J, Suvorov A, Araujo C, Rimashevskaya E, Pika T, Gaidano G, Weisel K, Goranova-Marinova V, Schwarer A, Minuk L, Masszi T, Karamanesht I, Offidani M, Hungria V, Spencer A, Orlowski RZ, Gillenwater HH, Mohamed N, Feng S, Chng WJ, and Investigators E (2016) Carfilzomib and dexamethasone versus bortezomib and dexamethasone for

patients with relapsed or refractory multiple myeloma (ENDEAVOR): a randomised, phase 3, open-label, multicentre study. *Lancet Oncol* **17:**27-38.

Dou QP and Zonder JA (2014) Overview of proteasome inhibitor-based anti-cancer therapies: perspective on bortezomib and second generation proteasome inhibitors versus future generation inhibitors of ubiquitin-proteasome system. *Curr Cancer Drug Targets* **14:**517-536.

Fang Y, Wang Z, Zhang T, Teague J, and Wang Z (2015) Contribution of epoxide hydrolase and cytochrome P450 (CYP) enzymes on oprozomib disposition. *AAPS 2015-W4315*.

Fretland AJ and Omiecinski CJ (2000) Epoxide hydrolases: biochemistry and molecular biology. *Chem Biol Interact* **129:**41-59.

Gill SS and Hammock BD (1980) Distribution and properties of a mammalian soluble epoxide hydrase. *Biochem Pharmacol* **29:**389-395.

Hamman JH, Enslin GM, and Kotze AF (2005) Oral delivery of peptide drugs: barriers and developments. *BioDrugs* **19:**165-177.

Hari P, Shain KH, Voorhees P, Gabrail N, Abidi M, Zonder J, Boccia R, Richardson PG, Neuman L, Wong H, Dixon S, and Prada CP (2015) Oprozomib (OPZ) and dexamethasone (DEX) in patients (PTS) with relapsed and/or refractory multiple myeloma (RRMM): Updated results from dose escalation in a Phase 1B/2, multicenter, open-label study. *Haematologica* **100:**254.

Harshbarger W, Miller C, Diedrich C, and Sacchettini J (2015) Crystal structure of the human 20S proteasome in complex with carfilzomib. *Structure* **23:**418-424.

Hassett C, Lin J, Carty CL, Laurenzana EM, and Omiecinski CJ (1997) Human hepatic microsomal epoxide hydrolase: comparative analysis of polymorphic expression. *Arch Biochem Biophy* **337:**275-283.

Hosagrahara VP, Rettie AE, Hassett C, and Omiecinski CJ (2004) Functional analysis of human microsomal epoxide hydrolase genetic variants. *Chem Biol Interact* **150:**149-159.

Infante JR, Mendelson DS, Burris HA, 3rd, Bendell JC, Tolcher AW, Gordon MS, Gillenwater HH, Arastu-Kapur S, Wong HL, and Papadopoulos KP (2016) A first-in-human dose-escalation study

of the oral proteasome inhibitor oprozomib in patients with advanced solid tumors. *Invest New Drugs* **34:**216-224.

Kisselev AF and Goldberg AL (2001) Proteasome inhibitors: from research tools to drug candidates. *Chem Biol* **8:**739-758.

Kitteringham NR, Davis C, Howard N, Pirmohamed M, and Park BK (1996) Interindividual and interspecies variation in hepatic microsomal epoxide hydrolase activity: studies with cis-stilbene oxide, carbamazepine 10, 11-epoxide and naphthalene. *J Pharmacol Exp Ther* **278:**1018-1027.

Kodani SD and Hammock BD (2015) The 2014 Bernard B. Brodie award lecture-epoxide hydrolases: drug metabolism to therapeutics for chronic pain. *Drug Metab Dispos* **43:**788-802.

Kroetz DL, Loiseau P, Guyot M, and Levy RH (1993) In vivo and in vitro correlation of microsomal epoxide hydrolase inhibition by progabide. *Clin Pharmacol Ther* **54:**485-497.

Kuhn DJ, Chen Q, Voorhees PM, Strader JS, Shenk KD, Sun CM, Demo SD, Bennett MK, van Leeuwen FW, Chanan-Khan AA, and Orlowski RZ (2007) Potent activity of carfilzomib, a novel, irreversible inhibitor of the ubiquitin-proteasome pathway, against preclinical models of multiple myeloma. *Blood* **110:**3281-3290.

Kumatori A, Tanaka K, Inamura N, Sone S, Ogura T, Matsumoto T, Tachikawa T, Shin S, and Ichihara A (1990) Abnormally high expression of proteasomes in human leukemic cells. *Proc Natl Acad Sci U S A* **87:**7071-7075.

Levy D (1996) Membrane proteins which exhibit multiple topological orientations. *Essays Biochem* **31:**49-60.

Li B and Dou QP (2000) Bax degradation by the ubiquitin/proteasome-dependent pathway: involvement in tumor survival and progression. *Proc Natl Acad Sci U S A* **97:**3850-3855.

Loda M, Cukor B, Tam SW, Lavin P, Fiorentino M, Draetta GF, Jessup JM, and Pagano M (1997) Increased proteasome-dependent degradation of the cyclin-dependent kinase inhibitor p27 in aggressive colorectal carcinomas. *Nat Med* **3:**231-234.

Moreau P, Masszi T, Grzasko N, Bahlis NJ, Hansson M, Pour L, Sandhu I, Ganly P, Baker BW, Jackson SR, Stoppa AM, Simpson DR, Gimsing P, Palumbo A, Garderet L, Cavo M, Kumar S, Touzeau C, Buadi FK, Laubach JP, Berg DT, Lin J, Di Bacco A, Hui AM, van de Velde H, Richardson PG, and Group T-MS (2016) Oral ixazomib, lenalidomide, and dexamethasone for multiple myeloma. *N Engl J Med* **374:**1621-1634.

Morisseau C, Beetham JK, Pinot F, Debernard S, Newman JW, and Hammock BD (2000) Cress and potato soluble epoxide hydrolases: purification, biochemical characterization, and comparison to mammalian enzymes. *Arch Biochem Biophys* **378:**321-332.

Morisseau C, Bernay M, Escaich A, Sanborn JR, Lango J, and Hammock BD (2011) Development of fluorescent substrates for microsomal epoxide hydrolase and application to inhibition studies. *Anal Biochem* **414:**154-162.

Morisseau C, Newman JW, Wheelock CE, Hill Iii T, Morin D, Buckpitt AR, and Hammock BD (2008) Development of metabolically stable inhibitors of mammalian microsomal epoxide hydrolase. *Chem Res Toxicol* **21:**951-957.

O'Connor OA, Wright J, Moskowitz C, Muzzy J, MacGregor-Cortelli B, Stubblefield M, Straus D, Portlock C, Hamlin P, Choi E, Dumetrescu O, Esseltine D, Trehu E, Adams J, Schenkein D, and Zelenetz AD (2005) Phase II clinical experience with the novel proteasome inhibitor bortezomib in patients with indolent non-Hodgkin's lymphoma and mantle cell lymphoma. *J Clin Oncol* **23:**676-684.

Obach RS (1999) Prediction of human clearance of twenty-nine drugs from hepatic microsomal intrinsic clearance data: An examination of in vitro half-life approach and nonspecific binding to microsomes. *Drug Metab Dispos* **27:**1350-1359.

Pacifici GM, Temellini A, Giuliani L, Rane A, Thomas H, and Oesch F (1988) Cytosolic epoxide hydrolase in humans: development and tissue distribution. *Arch Toxicol* **62:**254-257.

Pinarbasi H, Silig Y, and Pinarbasi E (2010) Microsomal epoxide hydrolase polymorphisms. *Mol Med Rep* **3:**723-727.

Rajan AM and Kumar S (2016) New investigational drugs with single-agent activity in multiple myeloma. *Blood Cancer J* **6:**e451.

Rose TE, Morisseau C, Liu JY, Inceoglu B, Jones PD, Sanborn JR, and Hammock BD (2010) 1-Aryl-3-(1-acylpiperidin-4-yl)urea inhibitors of human and murine soluble epoxide hydrolase: structure-activity relationships, pharmacokinetics, and reduction of inflammatory pain. *J Med Chem* **53:**7067-7075.

Shah J, Niesvizky R, Stadtmauer E, Rifkin RM, Berenson J, Berdeja JG, Sharman JP, Lyons R, Klippel Z, Wong H, Chang Y-L, and Usmani S (2015) Oprozomib, Pomalidomide, and Dexamethasone (OPomd) in Patients (Pts) with Relapsed and/or Refractory Multiple Myeloma (RRMM): Initial Results of a Phase 1b Study. *Blood* **126:**378-378.

Teague J, Wang Z, Jones J, Jiang J, Muchamuel T, Phizackerley K, Wong H, and Kirk C (2013) Understanding the absorption characteristics of the oral (PO) proteasome inhibitor oprozomib in the gastrointestinal (GI) tract. *AAPS 2013-000358*.

Thompson JL (2013) Carfilzomib: a second-generation proteasome inhibitor for the treatment of relapsed and refractory multiple myeloma. *Ann Pharmacother* **47:**56-62.

Vaclavikova R, Hughes DJ, and Soucek P (2015) Microsomal epoxide hydrolase 1 (EPHX1): Gene, structure, function, and role in human disease. *Gene* **571:**1-8.

Vij R, Savona M, Siegel D, Kaufman JL, Badros A, Ghobrial I, Paner A, Jagannath S, Jakubowiak A, Mikhael J, Kapoor P, Neuman L, Obreja M, and Berdeja J (2015) Updated results from a multicenter, open-label, dose-escalation phase 1B/2 study of single-agent oprozomib (OPZ) in patients (PTS) with hematologic malignancies, including multiple myeloma (MM). *Haematologica* **100:**251.

Wang Z, Yang J, Kirk C, Fang Y, Alsina M, Badros A, Papadopoulos K, Wong A, Woo T, Bomba D, Li J, and Infante JR (2013) Clinical pharmacokinetics, metabolism, and drug-drug interaction of carfilzomib. *Drug Metab Dispos* **41:**230-237.

Wienkers LC and Heath TG (2005) Predicting in vivo drug interactions from in vitro drug discovery data. *Nat Rev Drug Discov* **4:**825-833.

Yang J, Wang Z, Fang Y, Jiang J, Zhao F, Wong H, Bennett MK, Molineaux CJ, and Kirk CJ (2011) Pharmacokinetics, pharmacodynamics, metabolism, distribution, and excretion of carfilzomib in rats. *Drug Metab Dispos* **39:**1873-1882.

Zhou HJ, Aujay MA, Bennett MK, Dajee M, Demo SD, Fang Y, Ho MN, Jiang J, Kirk CJ, Laidig GJ, Lewis ER, Lu Y, Muchamuel T, Parlati F, Ring E, Shenk KD, Shields J, Shwonek PJ, Stanton T, Sun CM, Sylvain C, Woo TM, and Yang J (2009) Design and synthesis of an orally bioavailable and selective peptide epoxyketone proteasome inhibitor (PR-047). *J Med Chem* **52:**3028-3038.

Footnotes

The work was in part supported by the National Institute of Environmental Health Sciences grant [R01 ES002710].

Legends for Figures

Figure 1. Structures of carfilzomib and oprozomib. The numbers 1, 2, and 3 labeled on the structure indicate three possible cleavage sites of oprozomib by peptidases. PR-025 is the cleavage product containing an epoxyketone at site 1 of oprozomib.

Figure 2. *In vitro* metabolism of oprozomib in human hepatocytes. A) Representative ion chromatograms of oprozomib metabolites formed in human hepatocytes. Dash line: control sample, cell suspensions spiked with oprozomib; Solid line: cell suspensions after 1-hour incubation with oprozomib. B) Quantitative oprozomib (OPZ) disappearance and metabolite formation in human hepatocytes. At each time point, the levels of oprozomib, PR-176 and PR-025 diol in cell suspensions were quantified and then normalized as the percentage of initial oprozomib concentration at zero-minute. Data represent mean ± S.D. from three replicate incubations. PR-176 was the predominant metabolite formed via epoxide hydrolysis within one-hour incubation.

Figure 3. Epoxide hydrolysis by recombinant microsomal and soluble EHs. A) Epoxide hydrolysis of oprozomib by recombinant human mEH and sEH. Formation of PR-176 was quantified after incubation of oprozomib (2 μM) with various concentrations of enzymes for 30 min. A pilot study has shown a linear formation of PR-176 within 30 min under current conditions. B) Epoxide hydrolysis of *cis*-SO and *trans*-SO (50 μM) by mEH and sEH (5 μg/ml), respectively. Significant diol product formation was observed after incubation for 10 or 20 min, confirming the hydrolysis activities of EHs. C) Kinetics of the formation of PR-176 using recombinant mEH. A range of oprozomib concentrations were incubated with mEH (2 μg/ml) at 37 ^{o}C for 30 min. D) Kinetics of *cis*-SO hydrolysis using recombinant mEH. A series of *cis*-SO concentrations were incubated with mEH (4 μg/ml) at 37 °C for 10 min. Data represent mean ± S.D. from three replicate incubations. The K_m and V_{max} values were estimated by fitting the curve into the Michaelis-Menten equation.

Figure 4. Inhibition and kinetics of PR-176 formation in HLMs. A) Inhibition of mEH activity by NSPA in HLMs. Pooled HLMs (0.5 mg/ml) were incubated with oprozomib (10 μM) or *cis*-SO (50 μM) in the presence of various concentrations of NSPA at 37 °C for 15 min as indicated. The IC_{50} values were

estimated using nonlinear regression data analysis. B) Kinetics of PR-176 formation in male and female HLMs was conducted in 0.1 M potassium phosphate buffer (pH 7.4, 0.1 mg/ml BSA). Incubations were performed at 37 ^{o}C for 30 min. Data were fitted into the Michaelis-Menten equation for the calculation of K_m and V_{max} values. Data represent mean ± S.D. from triplicate incubations.

Figure 5. Inhibition of epoxide hydrolysis of oprozomib in human hepatocytes by the mEH inhibitor NSPA, but minimal inhibition by the sEH inhibitor TPPU. A) Percentage of oprozomib remaining in human hepatocytes. B) Formation of diol PR-176 in human hepatocytes. Cryopreserved human hepatocytes were incubated with oprozomib (2 μM) in the presence of NSPA, TPPU or vehicle 0.1% DMSO for various incubation times. Both oprozomib disappearance and PR-176 formation were quantified using LC-MS/MS. Data represent mean ± S.D. from triplicate incubations. The percentage of oprozomib was calculated using the remaining oprozomib concentration divided by zero-minute oprozomib concentration.

Figure 6. Metabolism of oprozomib by HLMs and recombinant CYPs. A) Percentage of oprozomib remaining in pooled HLMs in the presence or absence of cofactor NADPH. Initial oprozomib concentration was 1 μM. B) CYP phenotyping on oprozomib oxidation using six major CYP isoforms. Oprozomib was incubated with 6 recombinant CYP isoforms for various incubation times, individually. The loss of oprozomib was quantified using LC-MS/MS assays. Data represent mean ± S.D. from triplicate incubations.

Figure 7. Inhibition of CYP activities for oprozomib in human hepatocytes by 1-ABT. A) Percentage of oprozomib remaining in human hepatocytes. B) Formation of diol PR-176 in human hepatocytes. Cryopreserved human hepatocytes were incubated with oprozomib (2 μM) after pre-incubation with 1-ABT (0.5 mM) or 0.1% DMSO as vehicle for 30 min. Both oprozomib disappearance and PR-176 formation after various incubation times were quantified using LC-MS/MS. Data represent mean ± S.D. from triplicate incubations. The percentage of oprozomib was calculated using the remaining oprozomib concentration divided by zero-minute oprozomib concentration.

DMD Fast Forward. Published on April 20, 2017 as DOI: 10.1124/dmd.117.075226
This article has not been copyedited and formatted. The final version may differ from this version.

Scheme 1. Proposed major metabolic pathways of oprozomib in human hepatocytes. Oprozomib is predominantly metabolized by mEH in human hepatocytes, whereas CYPs, peptidases, and GST/GSH play minor roles. Oxidative and cleavage products containing an epoxyketone could be further metabolized via epoxide hydrolysis.

DMD Fast Forward. Published on April 20, 2017 as DOI: 10.1124/dmd.117.075226
This article has not been copyedited and formatted. The final version may differ from this version.

Table 1. ***In vitro*** **evaluation of oprozomib as an inhibitor of six human CYP enzymes.** Results representing the average data (i.e., percent of control activity) obtained from duplicate samples from each test article concentration were used to calculate IC_{50} values. The IC_{50} values were calculated using Graphpad Prism (v.5). The highest concentration of oprozomib tested in the assays was 30 µM.

Direct and time-dependent inhibition of human CYPs by oprozomib					
		Direct inhibition		Time-dependent inhibition	
		0-minute pre-incubation		30-minute pre-incubation	
Enzyme	CYP reaction	IC_{50} (µM)	Inhibition at 30 µM (%)[a]	IC_{50} (µM)	Inhibition at 30 µM (%)[a]
CYP1A2	Phenacetin *O*-deethylation	>30	21	>30	NA
CYP2C8	Amodiaquine *N*-dealkylation	>30	20	>30	13
CYP2C9	Diclofenac 4´-hydroxylation	>30	6.3	>30	24
CYP2C19	*S*-Mephenytoin 4´-hydroxylation	>30	16	>30	7.2
CYP2D6	Dextromethorphan *O*-demethylation	>30	0.2	>30	3.7
CYP3A4/5	Testosterone 6β-hydroxylation	>30	45	5.5	89
CYP3A4/5	Midazolam 1´-hydroxylation	>30	33	12	68

a: The inhibition (%) was calculated with the following formula and data for the highest concentration of test article evaluated: Inhibition (%) = 100% – percent activity remaining of solvent control.

NA: Not applicable. No value was obtained as the rates at the highest concentration of oprozomib evaluated (30 µM) were higher than the control rates.

DMD Fast Forward. Published on April 20, 2017 as DOI: 10.1124/dmd.117.075226
This article has not been copyedited and formatted. The final version may differ from this version.

Figure 1

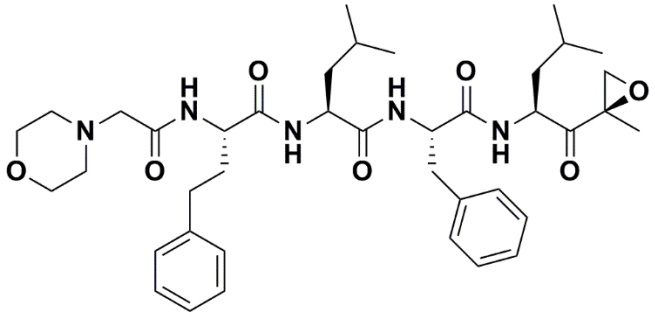

Carfilzomib

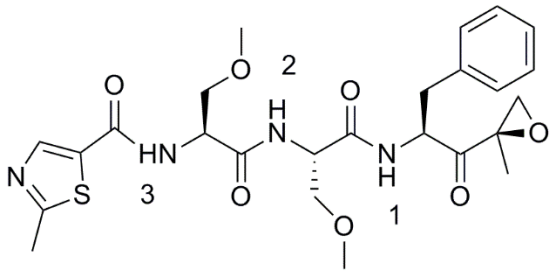

Oprozomib

DMD Fast Forward. Published on April 20, 2017 as DOI: 10.1124/dmd.117.075226
This article has not been copyedited and formatted. The final version may differ from this version.

Figure 2

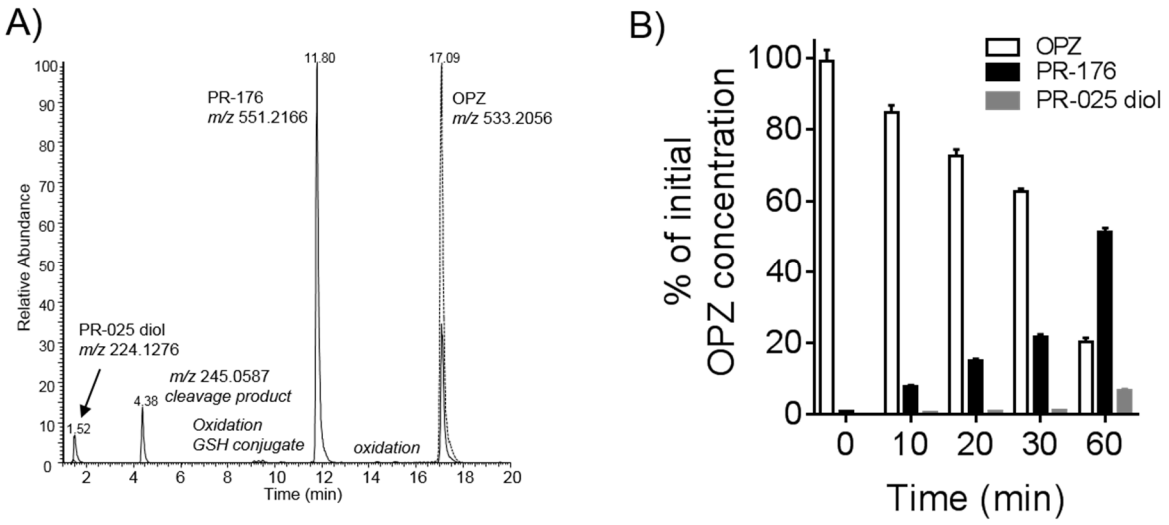

DMD Fast Forward. Published on April 20, 2017 as DOI: 10.1124/dmd.117.075226
This article has not been copyedited and formatted. The final version may differ from this version.

Figure 3

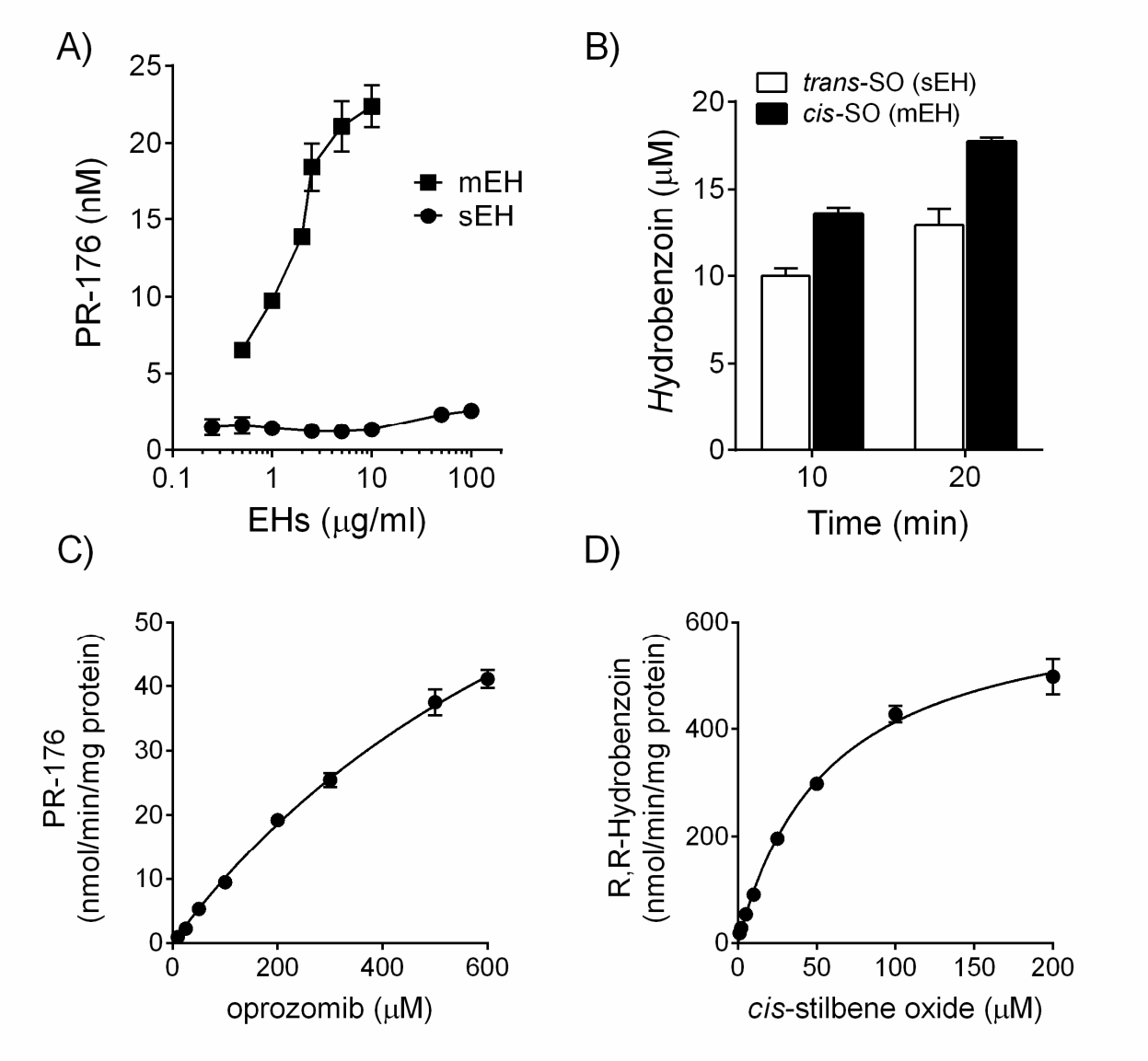

DMD Fast Forward. Published on April 20, 2017 as DOI: 10.1124/dmd.117.075226
This article has not been copyedited and formatted. The final version may differ from this version.

Figure 4

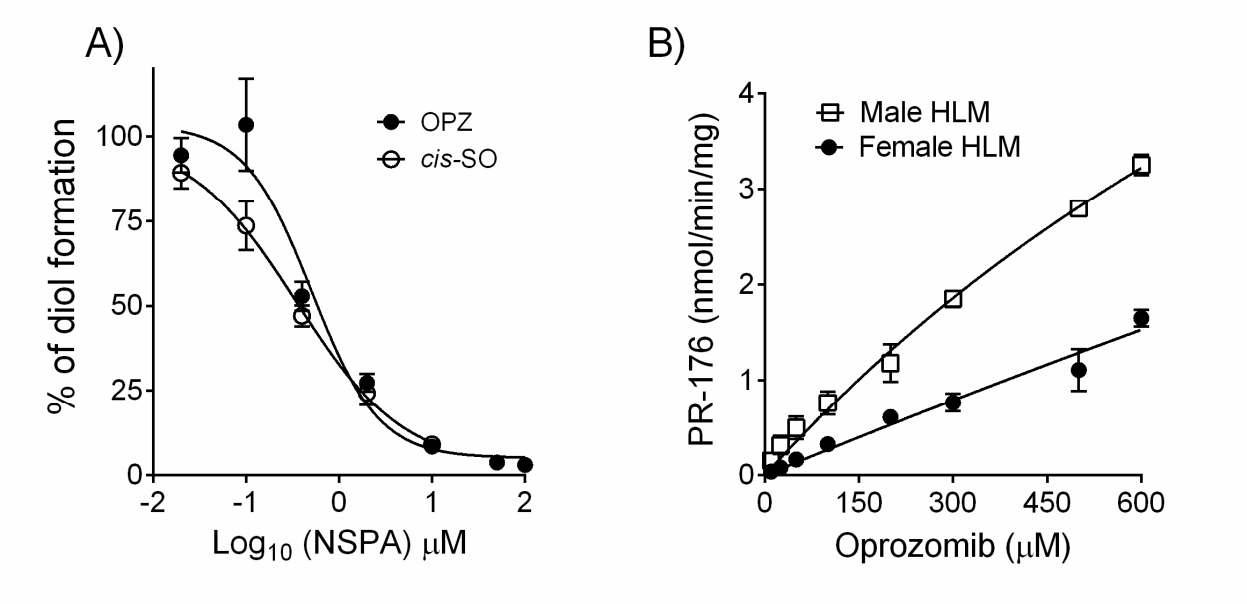

DMD Fast Forward. Published on April 20, 2017 as DOI: 10.1124/dmd.117.075226
This article has not been copyedited and formatted. The final version may differ from this version.

Figure 5

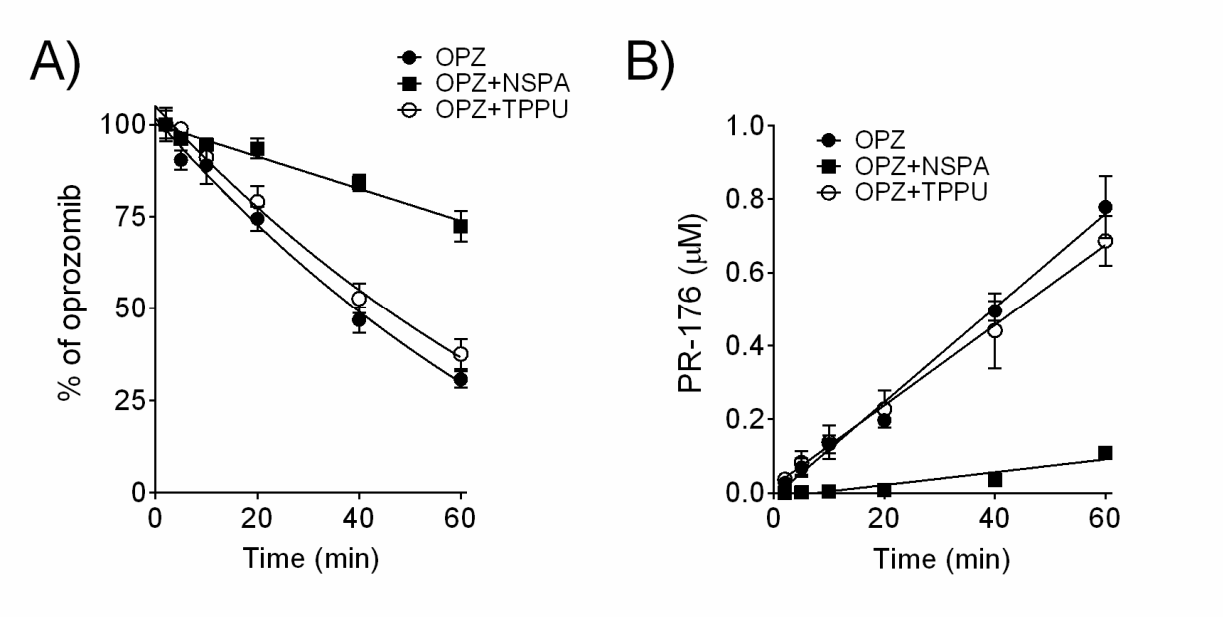

DMD Fast Forward. Published on April 20, 2017 as DOI: 10.1124/dmd.117.075226
This article has not been copyedited and formatted. The final version may differ from this version.

Figure 6

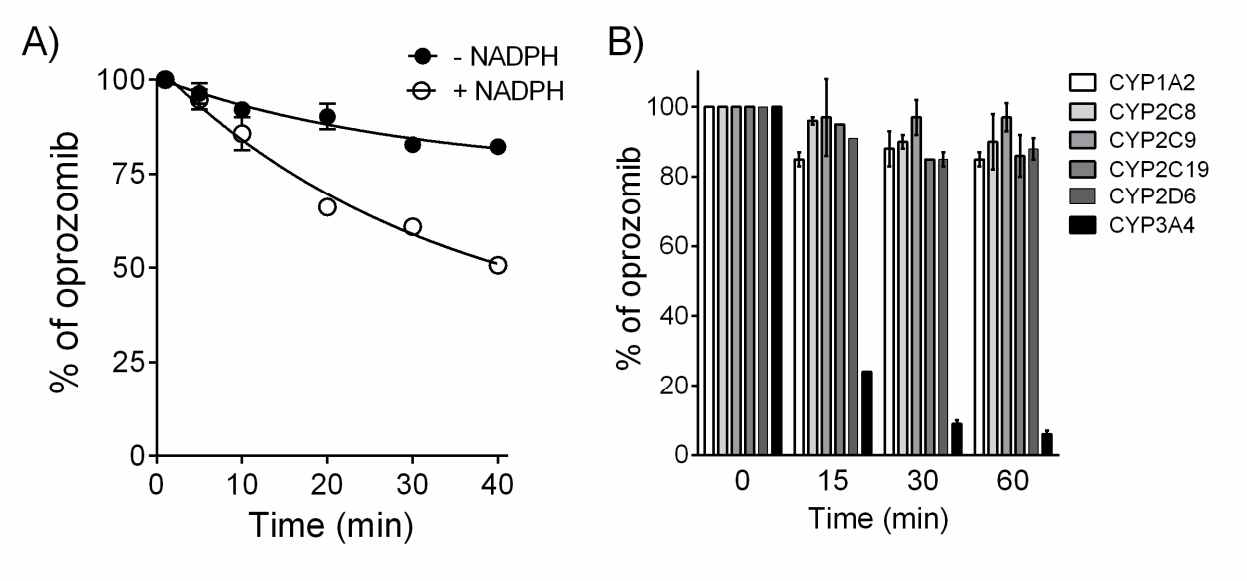

DMD Fast Forward. Published on April 20, 2017 as DOI: 10.1124/dmd.117.075226
This article has not been copyedited and formatted. The final version may differ from this version.

Figure 7

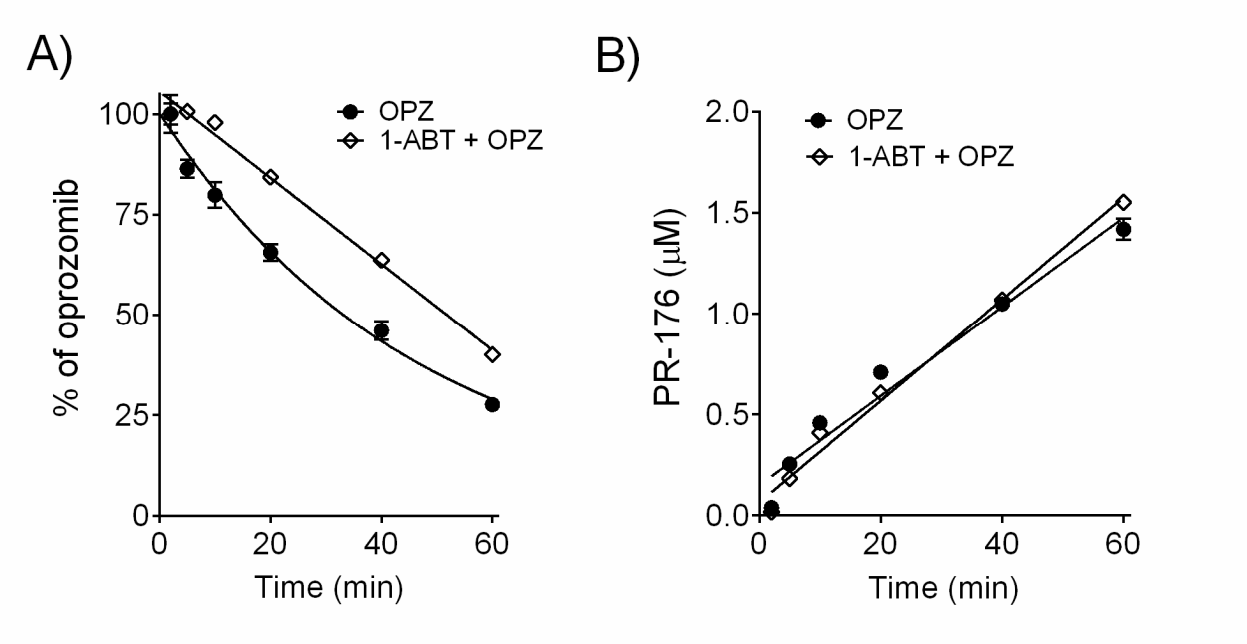

DMD Fast Forward. Published on April 20, 2017 as DOI: 10.1124/dmd.117.075226
This article has not been copyedited and formatted. The final version may differ from this version.

Scheme 1